PHYSICAL REVIEW C VOLUME 19, NUMBER 3 MARCH 1979

Converged values of second-order core-polarization diagrams with orthogonalized-plane-wave intermediate states

C. L. Kung and T. T. S. Kuo
Physics Department, State University of New York at Stony Brook, Stony Brook, New York 11794

K. F. Ratcliff
Physics Department, State University of New York at Albany, Albany, New York 12222

(Received 7 August 1978)

We carry out an extended study of the Vary-Sauer-Wong effect on the second-order core-polarization diagrams G_{3p1h} and G^T_{3p1h} in the effective interaction between two valence nucleons. As in Vary-Sauer-Wong, we first calculate G_{3p1h} using a harmonic oscillator propagator for the intermediate particle states p, including particle-hole excitations with energies up to $22\hbar\omega$. Results are in close agreement with those of Vary-Sauer-Wong. We then calculate G^T_{3p1h} where a free particle propagator for p is used. This is obtained by including the $-U$, the oscillator one-body potential, insertions of all orders to p of G_{3p1h}. Although the resulting matrix elements are generally smaller in magnitude than those of Vary-Sauer-Wong, the qualitative feature of the Vary-Sauer-Wong effect is clearly maintained. Namely there are strong cancellations between the contributions from the low and high energy p states. This makes the net effect from the core polarization diagrams significantly weaker than from G_{3p1h} calculated with $2\hbar\omega$ excitations alone. We also study some intermediate choices for the propagator of p, where the free particle propagator is used only for high energy valence states. The Brueckner reaction matrix elements in a mixed representation where one particle is in a harmonic oscillator state and the other in a plane wave state are needed in our calculations. By using the vector transformation brackets of Wong and Clement and of Balian and Brezin and the Tsai-Kuo treatment of the Pauli exclusion operator, we have developed a technique for accurately calculating these matrix elements.

[NUCLEAR STRUCTURE Contributions to effective interaction for $A=18$ nuclei calculated from converged values of lowest order core polarization diagrams as function of intermediate state propagator using new momentum space techniques.]

I. INTRODUCTION

The core-polarization diagram G_{3p1h} as shown in Fig. 1 has played a very important role in microscopic effective interaction theory, as pointed out some years ago by Bertsch[1] and by Kuo and Brown.[2] A primary function of this diagram is to provide[3] the much needed long range quadrupole-quadrupole component, the P_2 force, in the empirical effective interaction between valence nucleons. Since then, there have been many studies of the various aspects of this diagram.[4,5] The G_{3p1h} diagram is second order in G, the Brueckner reaction matrix. How important are the core-polarization diagrams (e.g., in Fig. 2) with higher orders in G? In the extensive calculations of Barrett and Kirson,[6] it was found that the core-polarization diagrams third order in G were of a magnitude comparable to G_{3p1h}. However, the inclusion of these higher order processes was found to result in poorer agreement with the empirical spectra of $A=18$ nuclei than had been achieved by Kuo-Brown. This raised a basic question about the convergence behavior of expanding the core-polarization process as a power series in G, and it has received extensive investigation.[7,4,5]

The issue of convergence of the effective interaction expansion in powers of G has been reopened in a fundamental way by the investigations of Vary, Sauer, and Wong.[8] Early calculations[1-3,6] of G_{3p1h} argued that the summation of the intermediate particle line p could be restricted by the energy condition $\epsilon_p-\epsilon_h=2\hbar\omega$ where the ϵ's are single particle energies of the particle p and hole h of G_{3p1h} (see Fig. 1) and $\hbar\omega$ is the harmonic oscillator energy spacing. We shall denote the contribution to G_{3p1h} from terms with $\epsilon_p-\epsilon_h=N\hbar\omega$ as $G_{3p1h}(N)$. Vary, Sauer, and Wong challenged the argument that G_{3p1h} could be adequately approximated by $G_{3p1h}(2)$. They performed the first converged calculation of G_{3p1h} by summing $G_{3p1h}(N)$ through $N=22$ for $A=18$ nuclei. They found a rather slow rate of convergence and could trace this to the dynamical effects of the tensor component of the Reid soft-core interaction. The net result was that the sum of $G_{3p1h}(N)$ for $N>4$ frequently has opposite sign from that of $G_{3p1h}(2)$ and therefore the resulting G_{3p1h} is considerably reduced in strength from the original $G_{3p1h}(2)$ estimate. No

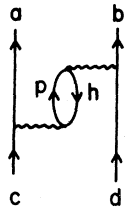

FIG. 1. The G_{3p1h} core-polarization diagram.

longer can the converged value of G_{3p1h} be claimed to provide all the long range quadrupole-quadrupole components indicated by the empirical effective interaction between valence nucleons. There is the further implication that the nonconverged values of diagrams higher than second order in G cannot be regarded as reliable evidence on the question of the convergence of the effective interaction in powers of the reaction matrix. Vary, Sauer, and Wong teach us that henceforth calculations of the effective interaction must guarantee adequate treatment of the dynamics of the nucleon-nucleon interaction.

The objective of the present work is to carry out an independent and extended investigation of the Vary-Sauer-Wong (VSW) effect. Our primary interest is to investigate the dependence of the converged value of G_{3p1h} upon the treatment of the intermediate particle state. To this end we present the results of four independent calculations of G_{3p1h} which are discussed in Sec. II. In parallel with VSW we first treat the intermediate particle state and propagator in harmonic oscillator representation, our main difference being in the treatment of the Pauli operator using the Tsai-Kuo[16] transformation rather than an angle-average approximation. At the other extreme we treat the intermediate particle state and propagator in plane wave representation and introduce techniques based on vector bracket transformations[14,15] that appear useful for the eventual calculation of higher order diagrams. These techniques are discussed in Sec. III. Finally we merge these approaches in two calculations in which low lying states are treated in oscillator representation whereas high lying intermediate particle states are treated in plane wave representation appropriately orthogonalized to the low lying states. Our results are presented and analyzed in Sec. IV.

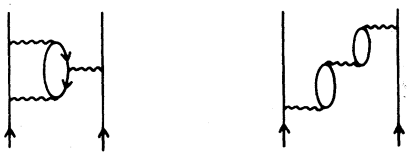

FIG. 2. Some core-polarization diagrams third order in G.

II. FORMULATION

When we include highly excited single particle states p in the calculation of the core-polarization diagram G_{3p1h}, the choice of representation for p and the self-energy insertions in the particle line become of particular interest. The many-body Hamiltonian is usually written as

$$H = H_0 + H_1 ,$$
$$H_0 = T + U , \tag{1}$$
$$H_1 = V - U ,$$

where T and V denote, respectively, the kinetic and potential energy of the many-body system under consideration. The auxiliary one-body potential U is introduced to yield a suitable unperturbed Hamiltonian H_0, the total Hamiltonian H being unaltered as a $-U$ term is then included in the interaction Hamiltonian H_1. We repeat the usual observation that if a complete evaluation of the series expansion were possible, the final answer would be found to be independent of our choice of U.

In treating low-lying nuclear states, the success of the nuclear shell model indicates that the choice of U as a harmonic oscillator potential

$$U = \sum_{i=1}^{A} \tfrac{1}{2} m\omega^2 r_i^{\,2} + C_0 \tag{2}$$

seems to be appropriate. This yields harmonic oscillator single particle states given by the solution of

$$H_0 \phi_i = \epsilon_i \phi_i \tag{3}$$

with $\epsilon_i = (2n_i + l_i + \frac{3}{2})\hbar\omega + C_0$. As it will be needed later for discussion of our results, we give a typical spectrum of this H_0 in Fig. 3. With this choice, the G_{3p1h} diagram of Fig. 1 may be written[6] as

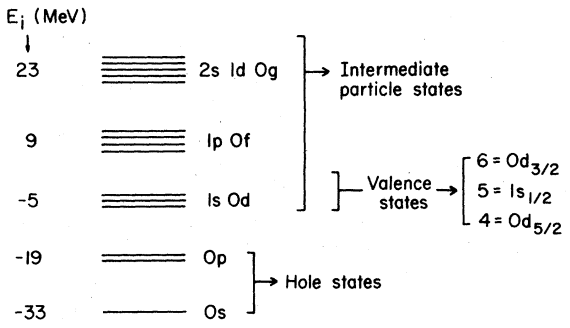

FIG. 3. The harmonic oscillator states and energies. Note that we have chosen the constant term C_0 of Eq. (2) as -54 MeV so that the energy of the valence states is -5 MeV. We use $\hbar\omega = 14$ MeV.

$$\langle abJT|G_{3p1h}|cdJT\rangle=(1+\delta_{ab})^{-1/2}(1+\delta_{cd})^{-1/2}\sum_{phJ_1J_2T_1T_2}(2J_1+1)(2J_2+1)(2T_1+1)(2T_2+1)\begin{Bmatrix}J_2 & j_p & j_a\\ j_h & J_1 & j_b\\ j_c & j_d & J\end{Bmatrix}$$
$$\times\begin{Bmatrix}T_2 & \frac{1}{2} & \frac{1}{2}\\ \frac{1}{2} & T_1 & \frac{1}{2}\\ \frac{1}{2} & \frac{1}{2} & T\end{Bmatrix}\langle hbJ_1T_1|G(\omega_f)|pdJ_1T_1\rangle\left\langle p\left|\frac{1}{\omega_0-H_0}\right|p\right\rangle$$
$$\times\langle apJ_2T_2|G(\omega_i)|chJ_2T_2\rangle\,, \tag{4}$$

with

$$\omega_f=\epsilon_c+\epsilon_d+\epsilon_h-\epsilon_a\,,$$
$$\omega_i=\epsilon_c+\epsilon_h\,,$$
$$\omega_0=\epsilon_c+\epsilon_d\,.$$

The energy ϵ for each state is given in Fig. 3, and the summation of the particle state p is over all the harmonic oscillator states except $0s$ and $0p$. The formula given above is only one of the four terms contained in G_{3p1h}, the other three being the diagrams obtained by exchanging ab, cd, and both ab and cd of the diagram shown in Fig. 1. In actual calculations, we of course include all the four terms. For the remainder of our discussion we will suppress all the factors in Eq. (4) except the last three matrix elements, remembering that these suppressed factors remain unchanged throughout the discussion.

We may remove the restriction over the summation p in Eq. (4) by introducing the one-particle projection operator $\hat{q}$ defined by

$$\hat{q}|n\rangle=|n\rangle,\quad \text{if } n>n_F$$
$$=0,\quad \text{if } n\leq n_F\,, \tag{5}$$

where n_F represents the "Fermi" energy level, namely the $0p_{1/2}$ orbit. In other words, $\hat{q}$ projects onto one particle oscillator states in the $1s0d$ shell and above. We can then rewrite Eq. (4), in abbreviated form, as

$$\langle ab|G_{3p1h}|cd\rangle$$
$$=\sum_{nn'h}\langle hb|G|nd\rangle\left\langle n\left|\frac{\hat{q}}{\omega_0-H_0}\right|n'\right\rangle\langle an'|G|ch\rangle\,. \tag{6}$$

The operator $\hat{q}/\omega_0-H_0$ is diagonal in the oscillator representation and therefore only terms with $n=n'$ would contribute in the evaluation of Eq. (6). With the particle summation unrestricted, we are then free to change the representation of the particle summation as we please. Thus in plane-wave representation of the intermediate state we would have

$$\langle ab|G_{3p1h}|cd\rangle=\int dk\int dk'\sum_h\langle hb|G|kd\rangle\left\langle k\left|\frac{\hat{q}}{\omega_0-H_0}\right|k'\right\rangle$$
$$\times\langle ak'|G|ch\rangle\,. \tag{7}$$

The operator $\hat{q}/(\omega_0-H_0)$ is no longer diagonal in the plane-wave representation of Eq. (7).

The question concerning the choice of the single particle spectrum in the calculation of G_{3p1h} is rather similar to that in the calculation of the bare Brueckner reaction matrix.[9] Because of the strong short range repulsions contained in the free nucleon-nucleon interaction V, it is necessary to make a partial summation of the V interactions between two nucleons to all orders. This leads to the reaction matrix interaction, to be denoted by a wavy line vertex. When using an oscillator single particle spectrum, the resulting reaction matrix is given as

$$G(\omega)=V+V\frac{Q}{\omega-H_0}G(\omega)\,, \tag{8}$$

where ω is the energy variable and Q is a two particle projection operator insuring that at least one of the two intermediate particle lines must be outside the chosen model space [see Fig. 4(a)]. Our choice of the model space will be discussed later. It may be noted that Q and H_0 commute. Detailed calculations of $G(\omega)$ defined according to Eq. (8) have been carried out by Barrett, Hewitt, and McCarthy.[10]

As indicated by Eq. (1), we add a one-body potential U to T to form a unperturbed Hamiltonian H_0. Thus we must subtract U from V to form the interaction Hamiltonian $H_1=V-U$, to insure that the total Hamiltonian H be unaltered. The reaction matrix of Eq. (8) corresponds to the use of a Ham-

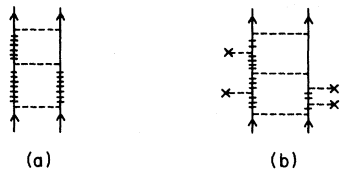

FIG. 4. Two-body ladder diagrams for the Brueckner reaction matrices G and G^T. Each railed line represents a single particle state which lies outside the chosen model space. The V interactions are represented by dotted lines (. . . .) and the $-U$ insertions by crosses (. . . . . x).

iltonian $H = H_0 + V$ instead of $H_0 + H_1$. In terms of diagrams, this $G(\omega)$ includes diagrams like Fig. 4(a). But it does not include the $-U$ insertions in diagrams such as the diagram of Fig. 4(b). One should have these $-U$ insertion diagrams, if the interaction Hamiltonian $H_1 = V - U$ is used. This point has been discussed by several authors.[11,12,9] The inclusion of these $-U$ insertions to all orders leads to a reaction matrix defined by

$$G^T(\omega) = V + VQ \frac{1}{\omega - QTQ} QG^T(\omega) , \tag{9}$$

where we note that Q and T do not commute. A detailed investigation of $G^T(\omega)$ has been carried out by Krenciglowa, Kung, Kuo, and Osnes.[9] In the above, ω is the energy variable. For the remainder of this paper we shall always understand by G that of Eq. (9) rather than that of Eq. (8).

The same argument about the $-U$ insertions may be applied to the calculation of the core-polarization diagram G_{3p1h}. This together with the consideration of being consistent with the calculation of $G^T(\omega)$ seems to strongly indicate that we should include the $-U$ insertions in the calculation of G_{3p1h}. To investigate this effect we then add $-U$ insertions to all orders to the particle line p of the G_{3p1h} diagram of Fig. 1, as illustrated by Fig. 5. These insertions lead to a geometric series of the form

$$-\frac{\hat{q}}{\omega_0 - H_0} U \frac{\hat{q}}{\omega_0 - H_0} + \frac{\hat{q}}{\omega_0 - H_0} U \frac{\hat{q}}{\omega_0 - H_0} U \frac{\hat{q}}{\omega_0 - H_0} - \cdots . \tag{10}$$

Together with G_{3p1h}, this series can be readily summed up and we obtain

$$\langle ab | G^T_{3p1h} | cd \rangle = \int dk \int dk' \sum_h \langle hb | G | kd \rangle \left\langle k \left| \hat{q} \frac{1}{\omega_0 - \hat{q}T\hat{q}} \hat{q} \right| k' \right\rangle \times \langle ak' | G | ch \rangle , \tag{11}$$

where we note that the connection between this equation and Eq. (7) for G_{3p1h} is very similar to that between $G^T(\omega)$ of Eq. (9) and $G(\omega)$ of Eq. (8).

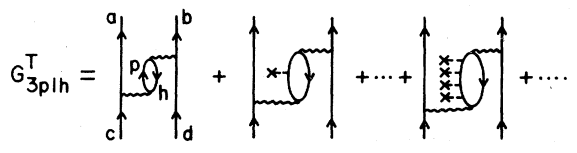

FIG. 5. Inclusion of the $-U$ insertions in the core polarization diagram G^T_{3p1h}. The first term in the series is G_{3p1h}.

We have used an abbreviated notation in Eq. (11). As the vertex $-U$ is inserted to the particle line p only, the operator $\omega_0 - \hat{q}T\hat{q}$ in fact means

$$\omega_0 - \hat{q}T\hat{q} \to \omega_0 - H_0' - \hat{q}t\hat{q} \equiv \omega_0' - \hat{q}t\hat{q} , \tag{12}$$

where H_0' operates on the intermediate states excluding p and the one-body kinetic energy operator t operates on p alone. For example, the G^T_{3p1h} diagram of Fig. 5 has $\omega_0' = (\epsilon_c + \epsilon_d) - (\epsilon_a + \epsilon_d - \epsilon_h)$. As was true in the transition from Eq. (8) to Eq. (9), the inclusion of $-U$ in H_1 to all orders has the effect of removing all dependence of the single particle propagator on our choice of U.

One may ask why we do not include the $-U$ insertions to the hole line h in G_{3p1h}. This is based on physical considerations. As is well known,[13] the Brueckner-Hartree-Fock (BHF) self-consistent single particle wave functions for the hole states ($0s_{1/2}$, $0p_{3/2}$ and $0p_{1/2}$) are well represented by harmonic oscillator wave functions. Thus the $-U$ insertions to the hole line in G_{3p1h} will be canceled, essentially, by the corresponding BHF self-energy insertions, as illustrated in Fig. 6. In fact, this type of cancellation may be reasonably expected for low-lying particle states such as those in the $0d$-$1s$ and even the $0f$-$1p$ shell.

The wave functions of particle states at higher excitation energies should not be expected to resemble those of the harmonic oscillator. In fact for very high excitation energy they should become well represented by free particle states. However, the exact choice of representation should not be crucial in the calculation of the converged value of G^T_{3p1h}, since the formalism merely instructs one to perform a complete intermediate particle sum subject only to the condition that these particle states be properly orthogonalized to the occupied low-lying states. This is ensured by exact treatment of the one-body projection operator $\hat{q}$ in Eq. (11). What is essential is that our inclusion of the $-U$ insertions from H_1 in the intermediate particle line, in parallel with the conventional treatment of G^T, has transformed the particle propagator into a form which is more easily handled in plane wave representation.

Physical considerations of the nature of the low-lying states suggests that one investigate treatment of the intermediate particle states as a compound spectrum. This idea is illustrated in Fig. 7. In Fig. 7(a) the entire intermediate particle

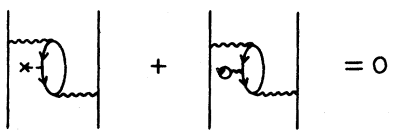

FIG. 6. Cancellation of hole-line $-U$ insertions.

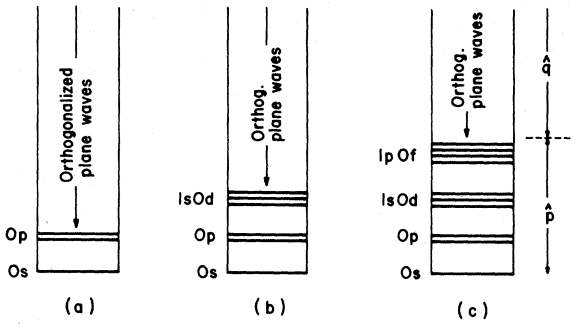

FIG. 7. Three choices of compound spectrum. The discrete states are those of a harmonic oscillator while the continuum states are plane waves made orthogonal to the former. The projectors for these two sets of states are denoted by $\hat{p}$ and $\hat{q}$, respectively.

sum is performed in plane wave representation properly orthogonalized to the occupied $0s$ and $0p$ orbitals. In Figs. 7(b) and 7(c) the intermediate particle sum is broken into two components. The first one or two excited major shells are treated in harmonic oscillator representation with a $1/\omega_0 - H_0$ propagator. The balance of the particle sum is then treated in plane wave representation as in Eq. (11) but with $\hat{q}$ orthogonalizing these plane waves to all states, both occupied and unoccupied, which have been treated in oscillator representation. In terms of the language introduced above, this compound spectrum approach corresponds to the exclusion of $-U$ insertions from low-lying states where Brueckner-Hartree-Fock considerations suggest cancellation of such insertions with self-energy bubbles, but inclusion of $-U$ insertions to all orders at energies above which BHF considerations should no longer be applicable. The results of all three choices of Fig. 7 in the calculation of G^T_{3p1h} will be reported in Sec. IV.

In summary then we present four separate converged calculations of the core-polarization diagram which differ from each other solely in the treatment of the propagator of the intermediate particle state. These range from the extreme of Eq. (6) in which all intermediate particle states are in oscillator representation to the extreme of Eq. (11) in which all are in plane-wave representation. However, in each case the pair of reaction matrices used in the core-polarization calculation are those of $G^T(\omega)$ of Eq. (9) in which the plane-wave propagator is used for the intermediate particle states. From a strictly formal point of view, we observe that it is in the calculation of G^T_{3p1h}, using Fig. 7(a) to define $\hat{q}$ in Eq. (11), that the intermediate particle propagators of $G^T(\omega)$ and those of the core-polarization diagrams are treated in identical manner. However, by using the same $G^T(\omega)$ in all four cases, our results focus clearly on the effect of choice of the single particle propagator on the converged value of the core-polarization diagram.

III. METHOD OF CALCULATION

The reaction matrix elements used in the evaluation of G^T_{3p1h} of Eq. (11) are of the form $\langle n_1 n_2 | G | k_3 n_4 \rangle$ where n_1, n_2, and n_4 are oscillator states and k_3 is a plane-wave state with δ-function normalization. Both bra and ket are antisymmeterized as indicated by our use of angular brackets. Since the use of such a "mixed representation" of plane wave and harmonic oscillator is somewhat unusual, we briefly abandon our condensed notation to express the familiar antisymmeterized, coupled, and normalized oscillator kets as a linear combination of uncoupled, product kets (denoted by rounded brackets) of the mixed representation:

$$|n_3 l_3 n_4 l_4 LM\rangle = \frac{1}{\sqrt{2}} \frac{1}{(1+\delta_{34})^{1/2}} \sum_{m_3 m_4} C^{l_3 l_4 L}_{m_3 m_4 M} i^{l_3} \int dk\, k\, P_{n_3 l_3}(k) [\,|k_3 l_3 m_3 n_4 l_4 m_4) - |n_4 l_4 m_4 k_3 l_3 m_3)\,], \tag{13}$$

where $P_{n_3 l_3}(k)$ is the radial wave function of the oscillator in momentum space representation

$$\langle \hat{k} | n_3 l_3 m_3 \rangle = \frac{1}{k} P_{n_3 l_3}(k) Y_{l_3 m_3}(\hat{k}); \tag{14}$$

which is related to the usual oscillator radial wave function $R_{n_3 l_3}(r)$ in coordinate space representation by

$$\frac{1}{r} R_{n_3 l_3}(r) = i^{l_3} \int dk \left(\frac{2}{\pi}\right)^{1/2} j_{l_3}(kr) k P_{n_3 l_3}(k). \tag{15}$$

Working backwards we arrive at the required matrix element $\langle n_1 n_2 | G | k_3 n_4 \rangle$ by transformation of the ket from pure plane wave representation

$$\langle n_1 n_2 | G | k_3 n_4 \rangle = \int dk_4 \langle n_1 n_2 | G | k_3 k_4 \rangle \langle k_4 | n_4 \rangle. \tag{16}$$

The coupling scheme actually used is of course that appropriate to a discussion of shell model orbitals

$$\langle n_1 n_2 | G | k_3 k_4 \rangle \rightarrow \langle n_1 l_1 j_1,\ n_2 l_2 j_2,\ JT | G | k_3 l_3 j_3, k_4 l_4 j_4, JT \rangle . \quad (17)$$

The calculation of these matrix elements in turn requires transformation into the two-body relative-center of mass (RCM) coordinate system. The transformation of the oscillator bra into RCM coordinates,

$$\langle n_1 l_1 j_1,\ n_2 l_2 j_2;\ JT | \rightarrow \langle nls(\mathcal{J})NL;\ JT | , \quad (18)$$

is accomplished by the well known Moshinsky transformation[9]

$$\langle n_1 l_1 j_1,\ n_2 l_2 j_2;\ JT | = \sum_{\lambda} \sum_{\substack{nlNL \\ S\mathcal{J}}} \frac{1-(-1)^{S+l+T}}{[2(1+\delta_{12})]^{1/2}} [(2j_1+1)(2j_2+1)(2\lambda+1)(2S+1)]^{1/2} \times \begin{Bmatrix} l_1 & l_2 & \lambda \\ \frac{1}{2} & \frac{1}{2} & S \\ j_1 & j_2 & J \end{Bmatrix} \langle nlNL\lambda | n_1 l_1 n_2 l_2 \lambda \rangle (2\lambda+1)(2\mathcal{J}+1)]^{1/2} W(\mathcal{J}LS\lambda;\ Jl) \langle nlS(\mathcal{J})NL;\ JT | , \quad (19)$$

where $\langle nlNL\lambda | n_1 l_1 n_2 l_2 \lambda \rangle$ is the Moshinsky bracket subject to angular momentum and energy conditions

$$\vec{l} + \vec{L} = \vec{\lambda} = \vec{l}_1 + \vec{l}_2 ,$$
$$(2n+l) + (2N+L) = (2n_1 + l_1) + (2n_2 + l_2) . \quad (20)$$

The transformation of the plane-wave ket into RCM coordinates

$$| k_3 l_3 j_3,\ k_4 l_4 j_4;\ JT \rangle \rightarrow | klS(\mathcal{J})KL;\ JT \rangle \quad (21)$$

is accomplished in parallel fashion by the less known vector bracket transformation[14,15]

$$| k_3 l_3 j_3,\ k_4 l_4 j_4; JT \rangle = \sum_{\mu} \sum_{lLS} \int dk \int dK \frac{1-(-1)^{S+l+T}}{\sqrt{2}} [(2j_3+1)(2j_4+1)(2\lambda+1)(2S+1)]^{1/2} \times \begin{Bmatrix} l_3 & l_4 & \lambda \\ \frac{1}{2} & \frac{1}{2} & S \\ j_3 & j_4 & J \end{Bmatrix} \langle klKL\lambda | k_3 l_3 k_4 l_4 \lambda \rangle [(2\mathcal{J}+1)(2\lambda+1)]^{1/2} W(\mathcal{J}LS\lambda;\ Jl) | klS(\mathcal{J})KL;\ JT \rangle , \quad (22)$$

where $\langle klKL\lambda | k_3 l_3 k_4 l_4 \lambda \rangle$ is the vector bracket subject to angular momentum and energy conditions

$$\vec{l} + \vec{L} = \vec{\lambda} = \vec{l}_3 + \vec{l}_4 ,$$
$$k^2 + \tfrac{1}{4}K^2 = \tfrac{1}{2}(k_3^2 + k_4^2) . \quad (23)$$

The vector bracket transformation has been extensively discussed by Wong and Clement.[15] For the purpose of numerical computation we find the formulation of the vector bracket given by Balian and Brezin[14] to be more convenient. We therefore use

$$\langle klKL\lambda | k_3 l_3 k_4 l_4 \lambda \rangle = 4\pi^2 \delta(w) \theta(1-x^2) A(x) , \quad (24)$$

where

$$w = k^2 + \tfrac{1}{4}K^2 - \tfrac{1}{2}(k_3^2 + k_4^2) ,$$
$$x = (k_3^2 - k^2 - \tfrac{1}{4}K^2)/kK ,$$
$$A(x) = \frac{1}{2\lambda+1} \sum_{\mu} [Y^l(\hat{k}) \times Y^L(\hat{K})]^{\lambda *}_{\mu} \times [Y^{l_3}(\hat{k}_3) \times Y^{l_4}(\hat{k}_4)]^{\lambda}_{\mu} . \quad (25)$$

We note that x is just the cosine of the angle between $\vec{k}$ and $\vec{K}$ and therefore the step function in Eq. (24) merely restricts x to its range of physical significance.

Since $A(x)$ is a scalar quantity, it can be calculated in any convenient coordinate system. The coordinate system we actually use is shown in

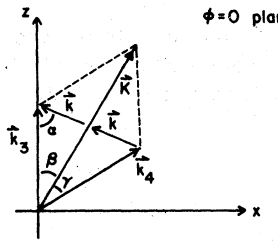

FIG. 8. Coordinate system used for evaluating vector transformation brackets.

Fig. 8. The z axis is chosen to be in the direction of $\vec{k}_3$ and the $\phi = 0$ plane is chosen to be the plane spanned by $\vec{k}_3$ and $\vec{k}_4$. The y axis is directed into the paper. In this way, $A(x)$ becomes

$$A(x) = \frac{(-1)^{l+L+\lambda}}{2\lambda+1} \sum_{\mu,M} (-1)^{\mu} C^{lL\lambda}_{mM-\mu} C^{l_3 l_4 \lambda}_{0\mu-\mu} Y^{l}_{m}(\alpha,0) \times Y^{L}_{M}(\beta,0) Y^{l_3}_{0}(0,0) Y^{l_4}_{\mu}(\gamma,0), \tag{26}$$

where

$$\alpha = \cos^{-1}\left[\frac{k_3^2 + k^2 - K^2/4}{2k k_3}\right],$$
$$\beta = \cos^{-1}\left[\frac{k_3^2 + K^2/4 - k^2}{k_3 k}\right], \tag{27}$$
$$\gamma = \cos^{-1}\left[\frac{k_3^2 + k_4^2 - 4k^2}{2k_3 k_4}\right].$$

We have found the vector transformation brackets depend on k and K quite smoothly thus being suitable for numerical integration techniques using momentum space Gaussian mesh points. (This numerical method was described in some detail in Ref. 9).

If we denote by MBT(...) and by VBT(...) the factors of the Moshinsky bracket transformation and of the vector bracket transformation of Eq. (19) and Eq. (22), respectively, then the transformation from the basic G-matrix elements to those needed in the calculation of G^T_{3p1h} in Eq. (11) can be realized in the following sequence of steps

$$\begin{aligned}
&\langle n_1 n_2 | G | k_3 n_4 \rangle \\
&= \int dk_4 \langle n_1 n_2 | G | k_3 k_4 \rangle \langle k_4 | n_4 \rangle \\
&= \sum \int dk_4 \mathrm{MBT}(\ldots)\mathrm{VBT}(\ldots) \\
&\quad \times \langle nlNL | G | k'l'K'L' \rangle \langle k_4 | n_4 \rangle \\
&= \sum \int dk_4 \int dk \int dK \langle klKL | G | k'l'K'L' \rangle \\
&\quad \times \langle n | k \rangle \langle N | K \rangle \langle k_4 | n_4 \rangle \mathrm{MBT}(\ldots) \\
&\quad \times \mathrm{VBT}(\ldots).
\end{aligned} \tag{28}$$

The basic input necessary to the calculation of mixed-representation matrix elements of G are those of RCM momentum space representation. These in turn are calculated by the Tsai-Kuo method[9,16] in which G is written exactly as the sum of two terms, G_F which is free of the two-body Pauli operator Q, and ΔG in which we have replaced Q by its complement P. If we set $e \equiv \omega - T$ then the G of Eq. (9) may be written as

$$G(\omega) = V + VQ\frac{1}{\omega - QTQ}QG(\omega) = G_F - \Delta G, \tag{29}$$

where

$$\begin{aligned}
G_F(\omega) &= V + V\frac{1}{e}G_F(\omega), \\
\Delta G &= G_F \frac{1}{e} P \frac{1}{P[1/e + (1/e)G_F(1/e)]P} P \frac{1}{e} G_F.
\end{aligned} \tag{30}$$

The single particle propagator of Eq. (11) in the calculation of G^T_{3p1h} can be handled by the Tsai-Kuo method in complete analogy to the above division of G. Denoting the single particle projection operators of Eq. (11) and Fig. (7) by $\hat{p} + \hat{q} = 1$ we have

$$\langle k | \hat{q} \frac{1}{\omega_0' - \hat{q}t\hat{q}} \hat{q} | k' \rangle = \langle k | \frac{1}{\omega_0' - t} | k' \rangle - \langle k | B | k' \rangle, \tag{31}$$

where

$$B \equiv \frac{1}{\omega_0' - t} \hat{p} \frac{1}{\hat{p}[1/(\omega_0' - t)]\hat{p}} \hat{p} \frac{1}{\omega_0' - t}. \tag{32}$$

In this way we express G^T_{3p1h} as the sum of two terms

$$\langle ab | G^T_{3p1h} | cd \rangle = (\text{direct term}) - (\text{Pauli term}), \tag{33}$$

where

$$\begin{aligned}
(\text{direct term}) &= \sum_h \int dk \langle hb | G | kd \rangle \\
&\quad \times \langle k | \frac{1}{\omega_0' - t} | k \rangle \langle ak | G | ch \rangle,
\end{aligned} \tag{34}$$

$$\begin{aligned}
(\text{Pauli term}) &= \sum_h \int dk \int dk' \langle hb | G | kd \rangle \\
&\quad \times \langle k | B | k' \rangle \langle ak' | G | ch \rangle.
\end{aligned} \tag{35}$$

In the direct term, Eq. (34), the propagation of the intermediate particle is uninhibited by the Pauli principle. The influence of occupied states upon the particle propagation is completely accounted for by the Pauli term, Eq. (35), and since $\hat{p}$ is a one-body operator this correction can be calculated exactly. In conclusion we note that such a division, achieved by $\hat{q} = 1 - \hat{p}$, in the calculation of G_{3p1h} with the oscillator propagator of Eq. (7) makes no sense due to the vanishing of the resulting energy denominators.

TABLE I. A detailed comparison of the contributions to some G_{3p1h} matrix elements. In each block the numbers in the the first line are the present values; second line, VSW's. Each G_{3p1h} matrix element is broken down according to the particle-hole excitation energy. The orbital notations 4, 5, and 6 of Fig. 3 are used.

	Particle–hole excitation energy									
TabcdJ	$2\hbar\omega$	$4\hbar\omega$	$6\hbar\omega$	$8\hbar\omega$	$10\hbar\omega$	$12\hbar\omega$	$14\hbar\omega$	$16\hbar\omega$	$18-22\hbar\omega$	Total
	−0.868	0.111	0.205	0.144	0.075	0.038	0.017	0.007	0.004	−0.267
144440	−0.710	0.126	0.205	0.144	0.081	0.040	0.018	0.007	0.004	−0.085
	0.153	0.147	0.181	0.169	0.118	0.065	0.029	0.011	0.005	0.878
155550	0.144	0.140	0.176	0.163	0.112	0.062	0.029	0.012	0.007	0.845
	−0.306	0.219	0.204	0.133	0.076	0.038	0.017	0.007	0.004	0.392
166660	−0.168	0.241	0.225	0.139	0.075	0.038	0.018	0.008	0.005	0.580
	−0.358	−0.079	0.035	0.057	0.041	0.027	0.014	0.007	0.004	−0.253
044441	−0.387	−0.083	0.034	0.058	0.046	0.028	0.014	0.007	0.004	−0.280
	0.238	0.102	0.035	0.025	0.020	0.014	0.008	0.004	0.003	0.449
045452	0.150	0.105	0.042	0.026	0.020	0.015	0.009	0.005	0.003	0.375
	0.403	0.246	0.106	0.039	0.010	−0.001	−0.004	−0.003	−0.003	0.794
046461	0.202	0.215	0.102	0.038	0.008	−0.002	−0.004	−0.003	−0.003	0.554
	0.276	0.180	0.099	0.062	0.037	0.022	0.011	0.006	0.003	0.696
046661	0.270	0.187	0.109	0.063	0.038	0.022	0.011	0.006	0.004	0.711
	0.132	0.099	0.085	0.064	0.040	0.021	0.009	0.004	0.001	0.456
055551	0.165	0.105	0.087	0.063	0.038	0.020	0.009	0.004	0.002	0.493
	0.238	0.053	0.055	0.082	0.075	0.055	0.033	0.017	0.011	0.618
055561	0.272	0.060	0.058	0.079	0.076	0.055	0.032	0.016	0.012	0.660
	−0.036	0.052	0.132	0.104	0.063	0.033	0.015	0.006	0.003	0.364
066661	0.007	0.061	0.135	0.108	0.064	0.033	0.015	0.006	0.004	0.432

TABLE II. Contributions to the $T = 1$ $1s0d$ shell G_{3p1h} matrix elements as functions of the particle-hole excitation energy.

	Particle–hole excitation energy in $\hbar\omega$										
TabcdJ	2	4	6	8	10	12	14	16	18	20	22
144440	−0.868	0.111	0.205	0.144	0.075	0.038	0.017	0.007	0.003	0.001	0.000
144442	0.066	0.088	0.088	0.062	0.033	0.017	0.008	0.004	0.001	0.000	0.000
144444	0.503	0.116	0.035	0.012	0.005	0.002	0.001	0.001	0.000	0.000	0.000
144452	−0.306	0.010	−0.018	−0.016	−0.007	−0.001	0.000	0.000	0.000	0.000	0.000
144462	0.100	−0.008	−0.001	−0.001	−0.002	−0.002	−0.002	−0.001	−0.000	−0.000	0.000
144464	−0.360	−0.032	−0.000	−0.000	−0.001	−0.000	0.000	0.000	0.000	0.000	0.000
144550	−0.383	−0.071	−0.032	0.013	0.025	0.020	0.011	0.005	0.002	0.001	0.000
144562	−0.354	−0.056	−0.020	−0.002	0.004	0.004	0.003	0.001	0.001	0.000	0.000
144660	−0.711	−0.070	0.023	0.025	0.015	0.007	0.003	0.001	0.000	0.000	0.000
144662	−0.402	−0.029	0.020	0.010	0.003	−0.000	−0.001	−0.000	−0.000	0.000	0.000
145452	−0.044	0.068	0.034	0.030	0.025	0.016	0.009	0.004	0.002	0.001	0.000
145453	0.670	0.160	0.059	0.029	0.015	0.008	0.004	0.002	0.001	0.000	0.000
145462	0.019	0.075	0.033	0.022	0.014	0.008	0.004	0.002	0.001	0.000	0.000
145463	−0.033	−0.002	0.006	0.007	0.005	0.002	0.001	0.000	0.000	0.000	0.000
145562	−0.121	−0.026	−0.033	−0.014	−0.001	0.003	0.003	0.002	0.001	0.000	0.000
145662	0.084	0.050	−0.000	−0.005	−0.001	0.001	0.001	0.001	0.000	0.000	0.000
146461	0.221	0.096	0.026	0.009	0.006	0.006	0.004	0.003	0.001	0.000	0.000
146462	0.229	0.145	0.076	0.035	0.016	0.007	0.004	0.002	0.001	0.000	0.000
146463	0.656	0.070	0.011	0.008	0.005	0.003	0.002	0.001	0.000	0.000	0.000
146464	0.596	0.128	0.041	0.013	0.004	0.002	0.001	0.001	0.000	0.000	0.000
146561	0.130	0.025	0.049	0.049	0.032	0.016	0.007	0.003	0.001	0.000	0.000
146562	−0.144	−0.009	−0.017	−0.014	−0.007	−0.002	0.000	0.000	0.000	0.000	0.000
146662	−0.230	0.005	0.032	0.026	0.016	0.008	0.004	0.002	0.001	0.000	0.000
155550	0.153	0.147	0.181	0.169	0.118	0.065	0.029	0.011	0.004	0.001	0.000
156560	−0.212	−0.097	−0.036	0.021	0.031	0.023	0.013	0.006	0.002	0.001	0.000
156561	0.722	0.124	0.037	0.016	0.009	0.005	0.003	0.001	0.001	0.000	0.000
156562	0.454	0.152	0.068	0.044	0.029	0.018	0.009	0.004	0.002	0.001	0.000
156662	−0.161	−0.012	−0.013	−0.004	0.001	0.003	0.002	0.001	0.001	0.000	0.000
166660	−0.306	0.219	0.204	0.133	0.076	0.038	0.017	0.007	0.003	0.001	0.000
166662	0.491	0.095	0.059	0.037	0.019	0.009	0.004	0.002	0.001	0.000	0.000

TABLE III. Contributions to the $T = 0$ $1s0d$ shell G_{3p1h} matrix elements as functions of the particle-hole excitation energy.

TabcdJ	$2\hbar\omega$	4	6	8	10	12	14	16	18	20	22
044441	−0.358	−0.079	0.035	0.057	0.041	0.027	0.014	0.007	0.003	0.001	0.000
044443	0.187	0.025	0.004	0.005	0.004	0.003	0.001	0.001	0.000	0.000	0.000
044445	−0.033	0.065	0.017	0.004	0.001	0.000	0.000	−0.000	0.000	0.000	0.000
044453	−0.176	−0.026	−0.004	−0.004	−0.003	−0.002	−0.001	−0.000	−0.000	0.000	0.000
044461	−0.108	−0.051	−0.008	0.008	0.008	0.005	0.002	0.001	0.000	0.000	0.000
044463	0.325	0.043	−0.010	−0.010	−0.004	−0.001	0.000	0.000	0.000	0.000	0.000
044551	−0.210	0.052	0.035	0.016	0.011	0.008	0.005	0.003	0.001	0.001	0.000
044561	−0.418	0.019	0.039	0.027	0.018	0.013	0.008	0.004	0.002	0.001	0.000
044661	−0.552	−0.028	0.006	0.001	−0.000	−0.001	−0.001	−0.001	−0.001	−0.000	−0.000
044663	0.312	0.057	−0.008	−0.009	−0.005	−0.003	−0.002	−0.001	−0.001	−0.000	−0.000
045452	0.238	0.102	0.035	0.025	0.020	0.014	0.008	0.004	0.002	0.001	0.000
045453	−0.301	−0.106	−0.032	−0.007	−0.002	−0.001	−0.001	−0.001	−0.000	−0.000	−0.000
045462	0.100	−0.007	−0.009	0.000	0.004	0.005	0.004	0.002	0.001	0.000	0.000
045463	−0.047	−0.013	0.004	0.001	0.000	0.001	0.001	0.001	0.001	0.000	0.000
045562	0.005	−0.053	−0.057	−0.035	−0.013	−0.001	0.002	0.002	0.001	0.001	0.000
045663	0.027	0.027	0.016	0.013	0.005	−0.001	−0.003	−0.002	−0.001	−0.001	−0.000
046461	0.403	0.246	0.106	0.039	0.010	−0.001	−0.004	−0.003	−0.002	−0.001	−0.000
046462	0.240	0.099	0.006	−0.010	−0.006	−0.001	0.001	0.001	0.001	0.000	0.000
046463	0.373	0.103	0.036	0.021	0.011	0.005	0.001	0.000	0.000	0.000	0.000
046464	0.143	0.004	0.011	0.004	0.000	−0.000	0.000	0.001	0.000	0.000	0.000
046551	−0.460	−0.074	−0.024	−0.013	−0.005	−0.000	0.001	0.001	0.001	0.000	0.000
046561	0.195	0.016	−0.028	−0.047	−0.044	−0.034	−0.021	−0.011	−0.005	−0.002	−0.001
046562	0.400	0.077	0.010	0.009	0.011	0.010	0.007	0.004	0.002	0.001	0.000
046661	0.276	0.180	0.099	0.062	0.037	0.022	0.011	0.006	0.002	0.001	0.000
046663	0.326	0.052	0.015	0.009	0.005	0.004	0.002	0.001	0.001	0.000	0.000
055551	0.132	0.099	0.085	0.064	0.040	0.021	0.009	0.004	0.001	0.000	0.000
055561	0.238	0.053	0.055	0.082	0.075	0.055	0.033	0.017	0.007	0.003	0.001
055661	0.305	0.009	−0.024	−0.038	−0.034	−0.025	−0.015	−0.007	−0.003	−0.001	−0.000
056561	0.215	−0.048	−0.044	−0.028	−0.019	−0.013	−0.009	−0.005	−0.003	−0.001	−0.000
056562	0.281	0.059	0.010	0.024	0.028	0.023	0.015	0.008	0.004	0.001	0.000
056661	−0.132	−0.038	0.019	0.013	0.003	−0.002	−0.002	−0.001	−0.001	−0.000	0.000
066661	−0.036	0.052	0.123	0.104	0.063	0.003	0.015	0.006	0.002	0.001	0.000
066663	0.080	0.055	0.022	0.007	0.003	0.001	0.001	0.000	0.000	0.000	0.000

IV. RESULTS AND DISCUSSIONS

We begin our discussion by a direct comparison of the results of the present calculation of G_{3p1h} in Eq. (6), using the oscillator propagator for the intermediate particle, with the corresponding results of VSW.[8] In Table I we list the contributions to each of the 10 matrix elements given by VSW arising from each value of the excitation energy of the intermediate particle-hole state. Our complete listing of the contributions for all $T = 1$ and $T = 0$ matrix elements is given, respectively, in Tables II and III.

Inspection of Table I reveals excellent agreement between the two calculations for contributions from high excitation energy. The differences are usually less than 10 per cent for 4–6 $\hbar\omega$ with even smaller differences for higher energies. However, the differences are seen to be quite significant for the $2\hbar\omega$ contribution. Indeed, differences in the totals are almost entirely attributable to this lowest energy contribution. Both VSW and the present calculation generate the necessary G-matrix elements from the Reid soft-core potential by solution of Eq. (9). However, the most significant difference we have been able to discern between these two calculations is in method of solution of Eq. (9).

We use the Tsai-Kuo procedure[16] as outlined in Eqs. (29) – (30). This procedure has been extensively investigated by Krenciglowa *et al.*[9] and in the language of that paper we have specifically used a (3,3,15) approximation to the correct (3,3,∞) version of the Pauli operator, Q, appropriate to G_{3p1h}. This should treat the Pauli operator with an overall accuracy of a few per cent. By contrast VSW use the angle-average approximation[11] to the (3,6,∞) version of Q. It would

TABLE IV. Complete breakdown values of 144440 G_{3p1h} matrix element. Note that contributions from particle states with a large l (g, h, i, j states) do not fall fast as we go to high n.

Hole state	Particle state	Quantum number n of the particle state							
nlj	lj	0	1	2	3	4	5	6	7
	$s_{1/2}$		0.022	0.002	0.001	0.001			
	$d_{3/2}$	−0.272	−0.021	0.001	0.001				
	$d_{5/2}$	−0.042	−0.000	−0.003	0.001				
$0s_{1/2}$	$g_{7/2}$	−0.007	−0.007	−0.003	−0.001				
	$g_{9/2}$	0.014	0.007	0.003	0.001	0.001			
	$i_{11/2}$	0.046	0.040	0.021	0.009	0.004	0.002	0.001	
	$p_{1/2}$		0.006	−0.003	−0.001				
	$p_{3/2}$		0.019	0.002	0.002	0.001			
	$f_{5/2}$	−0.303	−0.029	0.002	0.002	0.001			
$0p_{3/2}$	$f_{7/2}$	0.047	0.012	0.002					
	$h_{9/2}$	0.120	0.041	0.009	0.001				
	$h_{11/2}$	−0.003	−0.005	−0.004	−0.002	−0.001	−0.001		
	$j_{13/2}$	0.089	0.081	0.048	0.026	0.012	0.005	0.002	0.001
	$p_{1/2}$		−0.046	−0.001					
	$p_{3/2}$		−0.005	0.004	0.001				
$0p_{1/2}$	$f_{5/2}$	−0.299	−0.043	−0.004					
	$f_{7/2}$	0.006	−0.003	−0.001					
	$h_{9/2}$	0.041	0.008	0.001					
	$h_{11/2}$	0.025	0.018	0.011	0.006	0.003	0.002	0.001	

appear that the matrix elements of G, necessary to account for the low-lying contributions to G_{3p1h}, demand an accurate account of the Pauli operator. As expected, this sensitivity decreases rapidly with increasing excitation energy.

The important conclusion of VSW, that G_{3p1h} converges slowly with intermediate state excitation energy and that the $2\hbar\omega$ contribution alone is generally a poor approximation to the converged value of G_{3p1h}, is fully supported by our results. Additional insight into this conclusion may be gained from the example of the 144440 G_{3p1h} matrix element which is decomposed in Table IV into contributions arising from each particle-hole state considered separately. We call particular attention to the fact that the contributions from intermediate particle states with high values of l can be appreciable and fall off more slowly with increasing excitation energy than those with lower values of l. This behavior is consistent with VSW's conclusion that it is the tensor force which is responsible for the slow rate of convergence. The important contributions found to arise from particle states with $l = 6$, 7 will not begin to be accounted for until one has reached $6\hbar\omega$ in excitation energy.

It may be pointed out that a secondary purpose of the above G_{3p1h} calculation is to check our com-

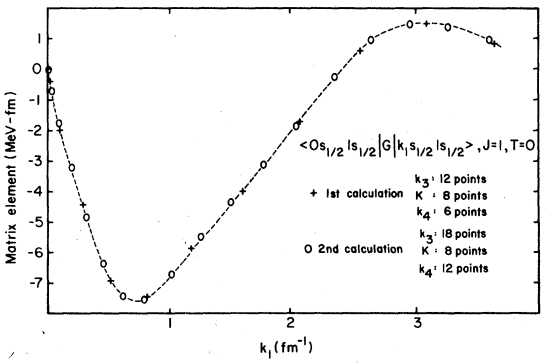

FIG. 9. Two calculations of $\langle 0s_{1/2}1s_{1/2}|G|ks_{1/2}1s_{1/2}\rangle$ $J=1$, $T=0$ matrix elements. The $\langle 0s_{1/2}1s_{1/2}|G|0s_{1/2}1s_{1/2}\rangle$ matrix element obtained by the first calculation is -1.745; the second, -1.754; and by the Moshinsky bracket transformation method, -1.758. k_3, k_4, and K are in the sense of Eq. (24).

puter codes. To our knowledge, the use of the vector transformation brackets in effective interaction calculations is probably first done in the present work. Thus it is necessary to make extensive checks, which we have done. In the above G_{3p1h} calculation, the matrix elements $\langle n_1 n_2 | G | n_3 n_4 \rangle$ used in Eq. (4) were in fact calculated via the vector transformation method. Namely we first calculate the mixed-representation matrix elements $\langle n_1 n_2 | G | k_3 n_4 \rangle$ as indicated by Eqs. (16) to (28). Then we perform the integration

$$\int dk_3 \langle n_1 n_2 | G | k_3 n_4 \rangle \langle k_3 | n_3 \rangle$$

to obtain $\langle n_1 n_2 | G | n_3 n_4 \rangle$. Hence the methods of computation used in VSW and in the present G_{3p1h} calculation are indeed quite different. The good agreement obtained between them, as indicated by Table I, thus lends strong support to the reliability of our calculations using the vector transformation brackets.

We turn next to the calculation of the mixed-representation matrix elements of G which are necessary in Eq. (11) for the calculation of G^T_{3p1h}. In Fig. 9 we show the behavior of $\langle 0s_{1/2} 1s_{1/2} | G | k_1 s_{1/2} 1s_{1/2} \rangle$ $J = 1$, $T = 0$ as a function of the intermediate particle momentum k_1. In the sense of Eq. (28) this matrix element was calculated as

$$\langle 0s_{1/2} 1s_{1/2} | G | k_1 s_{1/2} n_2 = 1 s_{1/2} \rangle = \int dk_2 \, \mathrm{VBT}(\ldots) \langle k_2 | n_2 \rangle = 1 \rangle \langle 0s_{1/2} 1s_{1/2} | G | kls(\mathcal{J}) KL \rangle, \tag{36}$$

where VBT(...) includes integration over k and K. The δ function in Eq. (24) for the vector bracket eliminates one of the four momenta as an independent variable. We eliminate the relative momentum k and thus for each value of k_1 must integrate over k_2 and K. Figure 9 shows the result of two completely different sets of Gauss mesh points used for these calculations. This typical smoothness of the matrix elements in their dependence on the momenta allows one to optimize the number of mesh points needed to economize the computation with minimal loss of accuracy. To illustrate the accuracy of the vector bracket transformation compared with that of the traditional Moshinsky bracket transformation we compute $\langle 0s_{1/2} 1s_{1/2} | G | 0s_{1/2} 1s_{1/2} \rangle$ by integration of Eq. (36), i.e.,

$$\langle 0s_{1/2} 1s_{1/2} | G | 0s_{1/2} 1s_{1/2} \rangle = \int dk_1 \langle k_1 | n_1 = 0 \rangle \langle 0s_{1/2} 1s_{1/2} | G | k_1 s_{1/2} 1s_{1/2} \rangle. \tag{37}$$

The smaller set of Gauss points yields a value of -1.745 MeV whereas the larger set of Gauss points gives -1.754 MeV to be compared with the value of -1.758 MeV achieved directly by Moshinsky transformation of the ket. This again serves as a check of our calculations using vector transformation brackets.

It is very instructive to compare the ways in which these G-matrix elements account for increasing particle excitation energy in the oscillator and plane-wave representations. In Fig. 10 we show two cases involving only s orbitals which should be dominated by the central force in the Reid soft-core potential. We display both G and G_F of Eq. (29) so that the effect of the Pauli operator as a function of particle momentum may be seen in the difference of G and G_F. We note that the large attractive elements of G for small values of the oscillator principal quantum number n are exactly paralleled by the low momentum behavior of G as is the change in sign of G with increasing n or k. In Figures 11(a) and 11(b) we

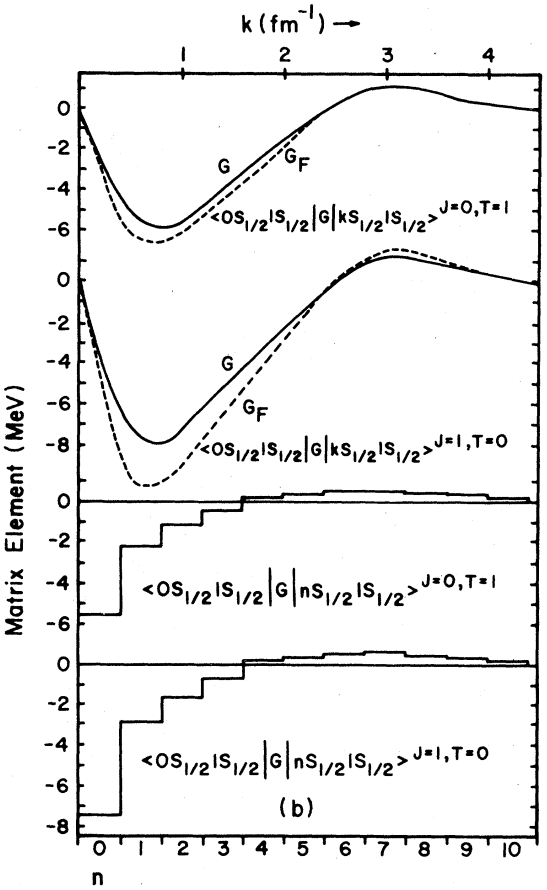

FIG. 10. Some of the G matrix elements due to the central forces: (a) The particle state is in momentum representation. (b) The particle state is in harmonic oscillator representation.

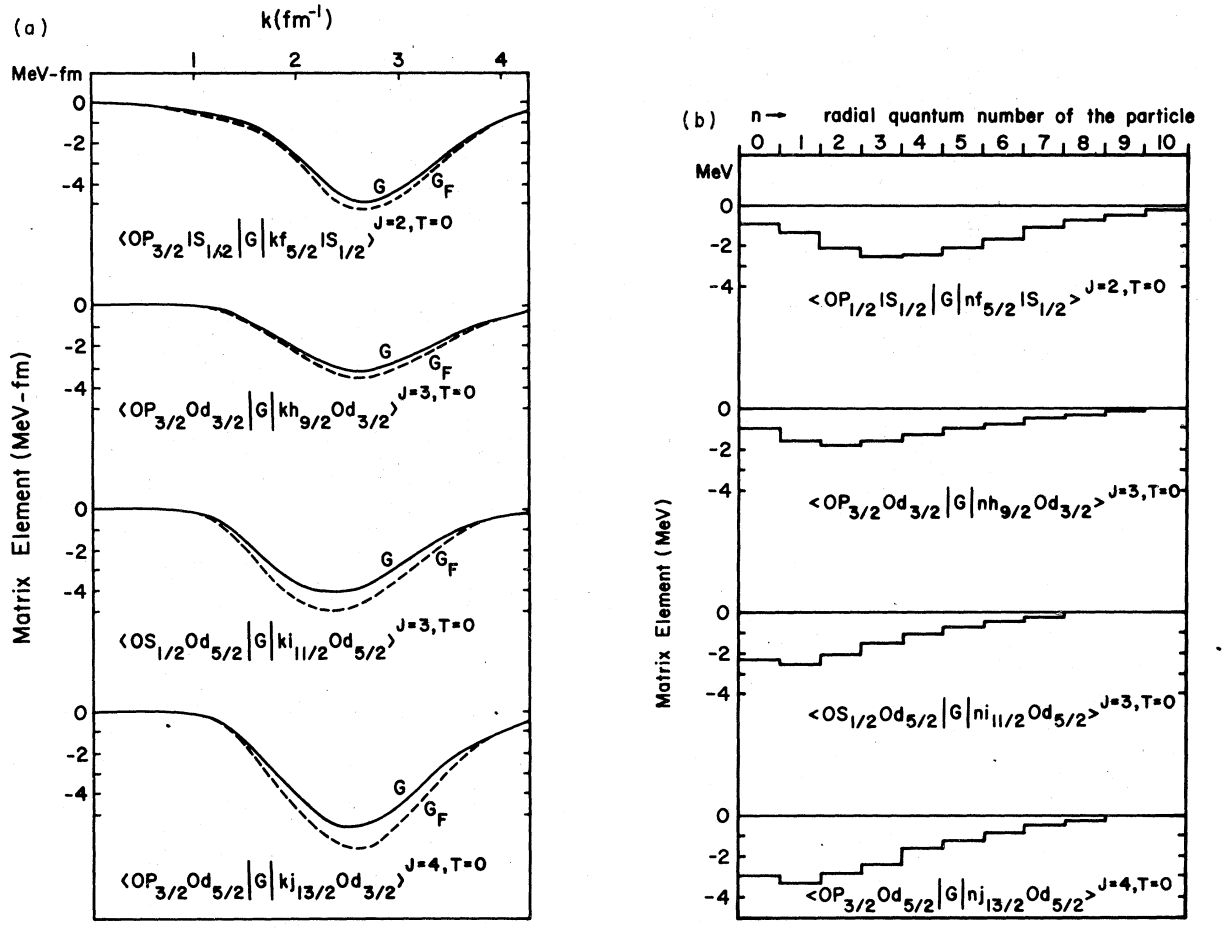

FIG. 11. Some of the G matrix elements due to the tensor force, the particle state is in momentum representation (a) and in oscillator representation (b).

show four matrix elements in which the particle state is characterized by a large value of the orbital angular momentum and should therefore be dominated by the tensor component of the Reid soft-core interaction. Collectively this group behaves very differently from those shown in Fig. 10. But again the behavior of G with increasing k parallels closely that with increasing n. In making the comparisons of Figures 11(a) and 11(b) it should be remembered that when l is large, even $n=0$ already indicates a sizeable excitation energy. Thus the long tail with increasing n in Fig. 11(b) or the concentration of the strength of G in the neighborhood of $k=3$ fm^{-1} in Fig. 11(a) are equivalent statements of the VSW effect that it is the dynamics of the interaction that will ultimately control the rate of convergence of the correlation of valence nucleons through core polarization. In other words, if we have a nucleon-nucleon potential which causes the G-matrix curves of Fig. 11(a) to peak at a much lower k value, then the contribution from the high energy particle states in the second order core-polarization diagram should be considerably reduced.

These matrix elements of G may then be combined in the fashion of Eqs. (33)–(35) to produce G^T_{3p1h}. We wish to analyze the dependence of G^T_{3p1h} on the momentum of the intermediate particle. To achieve this we rewrite Eqs. (33)–(35) as follows:

$$\langle ab\,|G^T_{3p1h}|\,cd\rangle = \int dk[DT(k) - PT(k)]\,, \tag{38}$$

where

$$\mathrm{DT}(k) = \sum_h \langle hb\,|G\,|kd\rangle\langle k\,|\frac{1}{\omega_0' - t}|\,k\rangle\langle ak\,|G\,|ch\rangle\,, \tag{39}$$

$$\mathrm{PT}(k) = \sum_h \int dk'\langle hb\,|G\,|kd\rangle\langle k\,|B\,|k'\rangle\langle ak'\,|G\,|ch\rangle\,, \tag{40}$$

TABLE V. The contributions to the $T = 1$ $1s0d$ shell of G^{T}_{3p1h} matrix elements as functions of the particle momentum.

	Particle momentum in fm^{-1}											
TabcdJ	0.022	0.114	0.278	0.511	0.810	1.169	1.584	2.046	2.548	3.082	3.640	4.212
144440	0.000	0.009	0.081	0.221	−0.171	−0.654	−0.163	0.355	0.289	0.093	0.011	0.000
144442	0.000	0.008	0.071	0.209	0.004	−0.134	0.121	0.186	0.128	0.045	0.006	0.000
144444	0.000	0.006	0.065	0.219	0.120	0.147	0.281	0.109	0.028	0.006	0.001	0.000
144452	0.000	0.000	0.002	−0.004	−0.071	−0.163	−0.085	−0.033	−0.036	−0.004	0.001	0.000
144462	0.000	0.001	−0.006	−0.026	0.049	0.089	−0.017	−0.004	0.002	−0.007	−0.002	−0.000
144464	0.000	0.001	0.006	0.006	−0.051	−0.204	−0.176	−0.030	−0.001	−0.001	0.000	0.000
144550	0.000	−0.000	−0.003	−0.026	−0.108	−0.273	−0.187	−0.057	0.040	0.054	0.009	0.000
144562	0.000	0.000	0.007	0.025	−0.059	−0.252	−0.187	−0.055	−0.004	0.013	0.003	0.000
144660	−0.000	−0.006	−0.043	−0.135	−0.177	−0.371	−0.387	0.004	0.075	0.021	0.002	0.000
144662	−0.000	−0.004	−0.028	−0.081	−0.091	−0.168	−0.183	0.006	0.025	−0.001	−0.001	0.000
145452	0.001	0.030	0.136	0.169	−0.064	−0.084	0.031	0.069	0.072	0.044	0.007	0.000
145453	0.001	0.039	0.192	0.320	0.107	0.175	0.311	0.175	0.076	0.025	0.004	0.000
145462	0.000	−0.001	−0.009	−0.027	−0.018	0.038	0.094	0.079	0.051	0.023	0.003	0.000
145463	0.000	−0.001	−0.004	0.002	0.002	−0.008	−0.005	0.000	0.014	0.007	0.001	0.000
145562	−0.000	−0.009	−0.058	−0.144	−0.068	−0.000	−0.018	−0.047	−0.037	0.009	0.003	0.000
145662	0.000	−0.002	−0.018	−0.066	−0.060	0.061	0.124	0.042	−0.010	0.004	0.002	0.000
146461	−0.000	−0.010	−0.036	−0.065	−0.128	0.194	0.331	0.091	0.021	0.019	0.005	0.000
146462	−0.000	−0.010	−0.028	−0.010	−0.052	0.191	0.333	0.168	0.079	0.022	0.004	0.000
146463	−0.000	−0.005	−0.005	0.039	0.086	0.392	0.350	0.060	0.018	0.010	0.002	0.000
146464	−0.000	−0.009	−0.032	−0.032	0.032	0.364	0.402	0.150	0.037	0.006	0.001	0.000
146561	0.000	0.002	0.008	0.012	0.040	0.047	0.031	0.083	0.121	0.046	0.005	0.000
146562	0.000	−0.002	−0.010	−0.032	−0.060	−0.071	−0.031	−0.021	−0.034	−0.005	0.001	0.000
146662	0.000	0.000	−0.006	−0.038	−0.071	−0.111	−0.086	0.039	0.068	0.025	0.003	0.000
155550	0.001	0.018	0.076	0.061	−0.068	0.021	0.153	0.305	0.426	0.193	0.023	0.001
155660	−0.000	−0.012	−0.071	−0.152	−0.033	0.005	−0.137	−0.120	0.050	0.071	0.013	0.001
156561	−0.000	−0.010	−0.016	0.052	0.067	0.387	0.459	0.148	0.042	0.015	0.003	0.000
156562	−0.000	−0.007	−0.014	0.022	0.009	0.218	0.338	0.193	0.114	0.057	0.009	0.000
156662	0.000	0.002	0.005	−0.010	−0.062	−0.108	−0.047	−0.020	−0.011	0.009	0.003	0.000
166660	−0.000	−0.003	0.000	−0.013	−0.232	−0.258	0.072	0.390	0.353	0.116	0.015	0.001
166662	−0.000	−0.005	−0.001	0.053	0.043	0.253	0.295	0.143	0.096	0.027	0.003	0.000

TABLE VI. The contributions to the $T = 0$ $1s0d$ shell of G^{T}_{3p1h} matrix elements as functions of the particle momentum.

	Particle momentum in fm^{-1}											
TabcdJ	0.022	0.114	0.278	0.511	0.810	1.169	1.584	2.046	2.548	3.082	3.640	4.212
044441	0.000	0.008	0.085	0.275	−0.005	−0.406	−0.205	0.004	0.121	0.073	0.012	0.001
044443	0.000	0.012	0.091	0.270	0.096	−0.124	0.056	0.026	0.011	0.007	0.001	0.000
044445	0.001	0.018	0.107	0.256	0.063	−0.269	−0.037	0.064	0.011	0.000	−0.000	0.000
044453	0.000	0.000	0.008	0.036	0.002	−0.107	−0.097	−0.025	−0.011	−0.007	−0.001	0.000
044461	0.000	0.002	0.013	0.029	−0.057	−0.162	−0.098	−0.020	0.025	0.015	0.001	0.000
044463	0.000	0.003	0.026	0.080	0.054	0.121	0.171	0.019	−0.024	−0.002	0.001	0.000
044551	0.000	0.000	0.005	0.010	−0.053	−0.112	−0.021	0.067	0.039	0.022	0.006	0.000
044561	0.000	0.000	0.006	0.013	−0.074	−0.211	−0.153	0.032	0.067	0.042	0.010	0.001
044661	0.001	0.015	0.090	0.196	−0.060	−0.460	−0.267	−0.036	−0.007	−0.005	−0.002	−0.000
044663	0.000	0.008	0.046	0.109	0.079	0.064	0.137	0.033	−0.022	−0.008	−0.002	−0.000
045452	0.001	0.037	0.204	0.406	0.051	−0.237	0.068	0.130	0.080	0.043	0.009	0.001
045453	0.000	0.012	0.068	0.155	0.001	−0.255	−0.213	−0.106	−0.026	−0.006	−0.003	−0.000
045462	0.000	−0.003	−0.020	−0.052	0.017	0.149	0.021	−0.029	0.007	0.018	0.006	0.000
045463	−0.000	−0.003	−0.021	−0.062	−0.031	0.061	−0.041	−0.014	0.009	0.005	0.003	0.000
045562	−0.001	−0.020	−0.129	−0.329	−0.126	0.209	0.072	−0.070	−0.081	−0.002	0.006	0.000
045663	−0.000	−0.005	−0.013	0.031	0.083	−0.039	−0.026	0.030	0.033	−0.004	−0.006	−0.001
046461	0.000	0.005	0.022	0.032	0.021	0.132	0.387	0.306	0.090	−0.008	−0.007	−0.001
046462	−0.000	−0.005	−0.042	−0.140	−0.053	0.262	0.242	0.063	−0.016	−0.002	0.003	0.000
046463	0.000	0.002	0.031	0.120	0.060	0.079	0.241	0.121	0.052	0.014	0.000	−0.000
046464	−0.001	−0.028	−0.145	−0.300	−0.121	0.331	0.216	0.026	0.013	−0.001	0.001	0.000
046551	0.000	0.000	−0.000	−0.015	−0.100	−0.244	−0.241	−0.088	−0.031	0.002	0.004	0.000
046561	0.000	0.005	0.033	0.119	0.163	0.008	0.026	−0.031	−0.126	−0.105	−0.025	−0.002
046562	−0.000	−0.003	−0.020	−0.054	0.004	0.256	0.269	0.081	0.028	0.033	0.009	0.001
046661	−0.000	−0.003	−0.006	−0.000	−0.053	0.039	0.261	0.259	0.176	0.068	0.012	0.001
046663	−0.000	−0.005	−0.012	0.008	0.008	0.131	0.204	0.076	0.028	0.011	0.003	0.000
055551	0.000	0.009	0.046	0.080	−0.016	−0.016	0.132	0.164	0.156	0.062	0.007	0.000
055561	0.000	0.009	0.026	−0.032	−0.079	0.104	0.194	0.127	0.201	0.178	0.037	0.002
055661	−0.000	−0.009	−0.038	−0.028	0.118	0.244	0.105	−0.025	−0.094	−0.078	−0.017	−0.001
056561	0.000	0.009	0.038	0.078	0.146	0.129	−0.030	−0.099	−0.074	−0.042	−0.012	−0.001
056562	−0.001	−0.013	−0.057	−0.102	−0.084	0.181	0.298	0.073	0.058	0.071	0.017	0.001
056661	0.000	−0.001	−0.004	−0.010	−0.014	0.009	−0.071	−0.023	0.025	−0.006	−0.003	−0.000
066661	−0.000	−0.011	−0.044	−0.071	−0.131	−0.002	0.093	0.190	0.260	0.099	0.013	0.001
066663	0.000	−0.001	−0.001	−0.002	−0.021	0.019	0.067	0.065	0.025	0.004	0.001	0.000

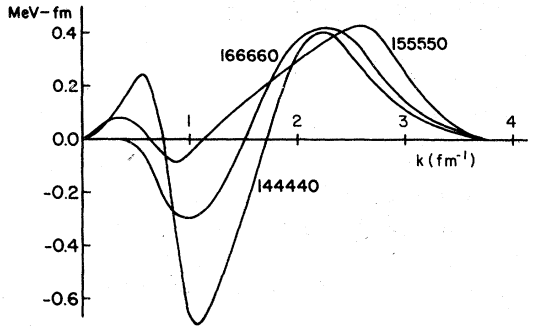

FIG. 12. The contributions to some G^T_{3p1h} matrix elements as a function of the particle momentum. It shows that the main contribution comes from moderate momentum components.

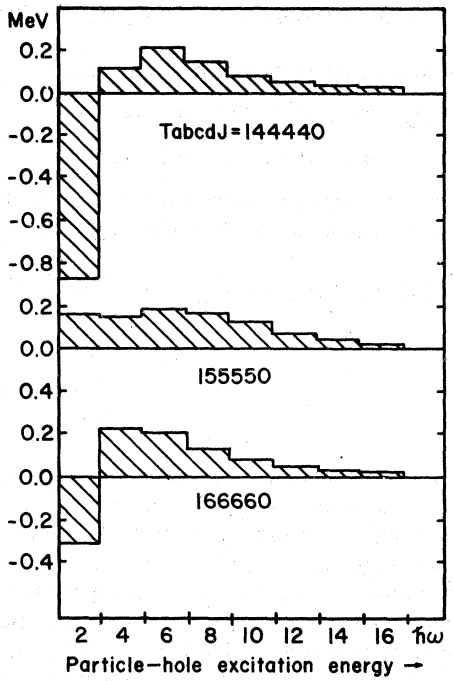

FIG. 13. The contribution to some G^T_{3p1h} matrix elements as a function of particle-hole excitation energy.

and B is defined in Eq. (32). Clearly DT(k) is just the integrand of the direct term in Eq. (34). Since B is not diagonal in plane-wave representation, the Pauli term in Eq. (35) is dependent in a symmetrical way upon a pair of wave numbers one of which must be integrated in order to express the Pauli term in terms of a PT(k) integrand which may be combined with DT(k). In Tables V and VI

TABLE VII. The particle-hole angular momentum breakdown. In each block the first number is for G_{3p1h}, and the second, G^T_{3p1h}. Each G_{3p1h} breakdown value is actually the sum of contributions from all particle states with various radial quantum numbers $n = 0, 1, 2\ldots$, and each G^T_{3p1h} breakdown value is the sum of the contributions from all the particle states with different momenta.

Hole states TabcdJ	Particle states						
144440	$s_{1/2}$	$d_{3/2}$	$d_{5/2}$	$g_{7/2}$	$g_{9/2}$	$i_{11/2}$	
$0s_{1/2}$	0.026	−0.291	−0.038	−0.017	0.026	0.122	
	0.012	−0.134	−0.016	−0.011	0.019	0.099	
	$p_{1/2}$	$p_{3/2}$	$f_{5/2}$	$f_{7/2}$	$h_{9/2}$	$h_{11/2}$	$j_{13/2}$
$0p_{3/2}$	0.003	0.025	−0.327	0.061	0.171	−0.017	0.264
	0.001	0.013	−0.165	0.032	0.128	−0.012	0.221
$0p_{1/2}$	−0.047	−0.000	−0.346	0.001	0.051	0.066	
	−0.027	−0.001	−0.176	0.003	0.039	0.049	
155550	$s_{1/2}$	$d_{3/2}$					
$0s_{1/2}$	−0.151	0.475					
	−0.065	0.293					
	$p_{1/2}$	$p_{3/2}$	$f_{5/2}$				
$0p_{3/2}$	0.108	0.045	0.300				
	0.057	0.029	0.201				
$0p_{1/2}$	−0.007	0.108					
	0.003	0.057					
166660	$s_{1/2}$	$d_{3/2}$	$d_{5/2}$	$g_{7/2}$			
$0s_{1/2}$	0.065	−0.032	0.044	0.068			
	0.028	−0.021	0.047	0.048			
	$p_{1/2}$	$p_{3/2}$	$f_{5/2}$	$f_{7/2}$	$h_{9/2}$		
$0p_{3/2}$	−0.023	0.124	0.068	−0.267	0.098		
	−0.009	0.059	0.035	−0.122	0.073		
$0p_{1/2}$	0.006	0.054	−0.012	0.200			
	0.005	0.027	−0.009	0.135			

we list the value of $DT(k) - PT(k)$ for 12 Gauss mesh points. These tables summarize the convergence behavior of the core-polarization diagram upon the excitation of the particle in plane-wave propagation in complete analogy to that of Tables III and IV for harmonic oscillator propagation. As an example we consider in Figs. 12 and 13 the behavior of three $T = 1$ matrix elements which exhibit slow convergence in both plane-wave (Fig. 12) and oscillator (Fig. 13) propagation. It is seen that the behavior shared by both 144440 and 166660 in the first $6\hbar\omega$ excitation is mirrored in their strong oscillation in the first 2 fm^{-1} of momentum space. By contrast the monotonic behavior of 155550 in oscillator space is reflected in a smoother behavior in k space with a concentration of strength in the neighborhood of 3 fm^{-1}. Despite these examples of similar behavior in the two representations and many others that can be extracted from Tables II, III, V and VI, it should be remembered that the oscillator wave functions are quite spread out in momentum space and thus sample the available excitation energy of the particle in very different ways. We may point to cases like 044445, 046464, and 055661 where the apparent rapid convergence in oscillator representation is seen to reflect strong cancellation when looked at in momentum representation.

A more detailed comparison of the three matrix elements compared in Figures 12 and 13 is given in Table VII, where the contribution to each of these is broken down according to the hole and angular momentum of the particle present in the intermediate particle-hole excitation. In each case the upper number refers to G_{3p1h} and represents therefore a sum over the principal quantum number n of the particle state. The lower number refers to contributions to G^T_{3p1h} and therefore represents an integration over k of the particle state fixing the value of l and j of this state. Arranged in this way the excellent correlations of the columns of Table VII in sign and relative magnitudes merely reflects the dynamical correlations of the Reid soft-core potential which are independent of the choice of intermediate state propagator. The comparison of different rows of Table VII reveals a general suppression of the contributions to G^T_{3p1h} relative to those to G_{3p1h} and this is principally reflecting the difference in the propagators in the two cases.

We further note a general suppression of the contributions in Table VII when the intermediate state has l and j quantum numbers identical with those of a hole state. These are the only angular momentum channels where the Pauli term, Eq. (35), will make a contribution to G^T_{3p1h}. In Table VIII we list separately the "direct term" of Eq. (34) and the "direct-Pauli term" of Eq. (33) as the first two rows of data in Table VIII. The last row repeats the contribution to G_{3p1h} of Table VII. We see that the direct term is very large and that the cancellation between direct and Pauli terms is almost complete as reflected in the smallness of the second row of numbers. (Note that the numbers in the last row are also quite small, and hence similar cancellation also takes place for G_{3p1h}.) Application of the Tsai-Kuo procedure in Eq. (31) allows exact treatment of the one-body Pauli operator and Table VIII shows that exact treatment is important in this case.

We turn next to a summary of all the various calculations of the sd-shell matrix elements of the effective interaction which are listed in Tables IX and X for $T = 1$ and $T = 0$, respectively. In order, we show in the first three columns the calculations of G_{3p1h} of Eq. (6) in which the intermediate particle sum is truncated by retaining

TABLE VIII. Cancellation of the direct and Pauli terms [see Eq. (33)] when the particle is in s or p states. In each block the numbers shown are (1) direct terms of G^T_{3p1h}, (2) net values of G^T_{3p1h}, (3) net values of G_{3p1h}. Note that the net values (for either G_{3p1h} or G^T_{3p1h}) are very small compared with the direct terms, so we say that the direct term and Pauli term are largely cancelled when particle is in s or p state.

TabcdJ	Hole state	Particle states		
		$s_{1/2}$	$p_{1/2}$	$p_{3/2}$
		−0.571		
	$0s_{1/2}$	0.012		
		0.026		
			−0.194	−0.980
144440	$0p_{3/2}$		0.001	0.013
			0.003	0.025
			−1.068	−0.159
	$0p_{1/2}$		−0.027	−0.001
			−0.047	0.000
		−0.638		
	$0s_{1/2}$	−0.065		
		−0.151		
			0.409	−0.933
155550	$0p_{3/2}$		0.057	0.029
			0.108	0.045
			−0.344	0.409
	$0p_{1/2}$		0.003	0.057
			−0.007	0.108
		−0.317		
	$0s_{1/2}$	0.028		
		0.065		
			−0.165	−1.435
166660	$0p_{3/2}$		−0.009	0.059
			−0.023	0.124
			−0.147	−0.091
	$0p_{1/2}$		0.005	0.027
			0.006	0.054

TABLE IX. The $T = 1$ three-particle–one-hole core-polarization matrix elements for the $1s0d$ shell.

	1	2	3	4	5	6	7	8
			G_{3p1h}			Compound spectra		
	$2\hbar\omega$	$2\hbar\omega$	$2\hbar\omega$	All	All	Fig.	Fig.	
TabcdJ	Kuo	VSW	present	VSW	present	7(c)	7(b)	G^T_{3p1h}
144440	−0.731	−0.710	−0.868	−0.085	−0.267	−0.392	−0.091	0.074
144442	0.061	0.054	0.066	0.349	0.367	0.301	0.247	0.259
144444	0.402	0.422	0.503	0.600	0.675	0.634	0.450	0.364
144452	−0.235	−0.210	−0.306	−0.241	−0.336	−0.324	−0.203	−0.161
144462	0.055	0.065	0.100	0.056	0.082	0.085	0.104	0.028
144464	−0.294	−0.283	−0.360	−0.313	−0.394	−0.386	−0.260	−0.186
144550	−0.242	−0.225	−0.383	−0.249	−0.408	−0.381	−0.207	−0.203
144562	−0.243	−0.269	−0.354	−0.327	−0.420	−0.397	−0.278	−0.211
144660	−0.572	−0.597	−0.711	−0.583	−0.707	−0.721	−0.388	−0.365
144662	−0.249	−0.369	−0.402	−0.365	−0.399	−0.408	−0.258	−0.189
145452	−0.034	−0.040	−0.044	0.154	0.143	0.103	0.105	0.135
145453	0.462	0.523	0.670	0.798	0.948	0.874	0.647	0.509
145462	0.015	0.060	0.019	0.222	0.177	0.136	0.123	0.120
145463	−0.025	−0.013	−0.033	0.010	−0.014	−0.017	0.002	0.006
145562	−0.059	−0.031	−0.121	−0.100	−0.187	−0.162	−0.095	−0.116
145662	0.043	0.127	0.084	0.177	0.131	0.120	0.094	0.055
146461	0.209	0.205	0.221	0.337	0.372	0.333	0.143	0.221
146462	0.210	0.216	0.229	0.505	0.514	0.437	0.281	0.330
146463	0.537	0.513	0.656	0.611	0.756	0.735	0.491	0.388
146464	0.413	0.604	0.596	0.806	0.787	0.735	0.519	0.408
146561	0.071	0.108	0.130	0.293	0.311	0.259	0.219	0.181
146562	−0.091	−0.106	−0.144	−0.158	−0.193	−0.176	−0.156	−0.102
146662	−0.197	−0.191	−0.230	−0.098	−0.135	−0.168	−0.097	−0.046
155550	0.146	0.144	0.153	0.845	0.878	0.668	0.557	0.575
155660	−0.135	−0.121	−0.212	−0.162	−0.247	−0.219	−0.127	−0.111
156561	0.546	0.604	0.722	0.811	0.918	0.873	0.613	0.487
156562	0.334	0.422	−0.454	0.757	0.780	0.692	0.558	0.427
156662	−0.119	−0.099	−0.161	−0.115	−0.181	−0.170	−0.110	−0.094
166660	−0.312	−0.168	−0.306	0.580	0.392	0.171	0.263	0.296
166662	0.414	0.429	0.491	0.670	0.717	0.652	0.439	0.390

only the $2\hbar\omega$ excitation. These results are, respectively, those of Kuo,[3] VSW,[8] and the present calculation. The converged values of the oscillator sum for G_{3p1h} of VSW and the present calculation are displayed in columns 4 and 5 of Tables IX and X. In columns 6 and 7 we present the results of the compound spectra treatment of the intermediate particle state as was discussed in Sec. II and illustrated in Fig. 7. Finally in column 8 we tabulate the results for G^T_{3p1h} of Eq. (11) in which all intermediate particle states are treated in plane-wave propagation.

To be specific concerning the compound spectra calculations, the results of column 7 in Tables IX and X are computed in the following manner: We compute G_{3p1h} according to Eq. (4) but the sum over the intermediate particle states is restricted to the three orbitals of the $1s$-$0d$ shell. To this partial sum for G_{3p1h} we add G^T_{3p1h} computed according to Eqs. (33)–(35) but with the single particle projection operator $\hat{p}$ in Eq. (32) now projecting onto the six orbitals of the $0s$, $0p$ and $1s$-$0d$ shells. In this way the intermediate plane-wave sum for the highly excited states in G^T_{3p1h} is properly orthogonalized to both the core states as well as the low-lying valence states we have chosen to treat in oscillator representation. The results of column 6 in Tables IX and X are computed in like manner except that the four orbitals of the $1p$-$0f$ shell are now also included in the partial sum for G_{3p1h} and therefore in the definition of $\hat{p}$ used in the computation of G^T_{3p1h} which is then added to G_{3p1h}.

The overall effect of the core-polarization diagram can be most easily summarized by looking at the shifts in the centroids of various TJ groups of levels due to the inclusion of core polarization. For example, some shifts in centroid

TABLE X. The $T = 0$ three-particle–one-hole-core-polarization matrix elements for the $1s0d$ shell.

	1	2	3	4	5	6	7	8
			G_{3p1h}			Compound spectra		
	$2\hbar\omega$	$2\hbar\omega$	$2\hbar\omega$	All	All	Fig.	Fig.	
TabcdJ	Kuo	VSW	present	VSW	present	7(c)	7(b)	G^T_{3p1h}
044441	−0.251	−0.387	−0.358	−0.280	−0.253	−0.256	−0.132	−0.046
044443	0.092	0.111	0.187	0.146	0.231	0.228	0.169	0.123
044445	−0.087	−0.108	−0.033	−0.026	0.053	0.032	0.060	0.029
044453	−0.141	−0.194	−0.176	−0.236	−0.217	−0.204	−0.142	−0.095
044461	−0.058	−0.021	−0.108	−0.039	−0.143	−0.137	−0.072	−0.102
044463	0.235	0.297	0.325	0.330	0.344	0.344	0.245	0.163
044551	−0.146	−0.208	−0.210	−0.077	−0.079	−0.114	−0.028	0.002
044561	−0.274	−0.384	−0.418	−0.252	−0.287	−0.330	−0.179	−0.089
044661	−0.496	−0.535	−0.552	−0.553	−0.578	−0.572	−0.413	−0.269
044663	0.206	0.242	0.312	0.276	0.340	0.337	0.210	0.148
045452	0.102	0.150	0.238	0.375	0.449	0.393	0.308	0.241
045453	−0.267	−0.342	−0.301	−0.502	−0.452	−0.398	−0.356	−0.205
045462	0.088	0.059	0.100	0.064	0.102	0.100	0.085	0.057
045463	−0.042	−0.006	−0.047	−0.016	−0.050	−0.058	−0.017	−0.023
045562	0.124	0.095	0.005	−0.061	−0.147	−0.104	−0.083	−0.119
045663	−0.049	−0.009	0.027	0.044	0.080	0.062	0.056	0.032
046461	0.207	0.202	0.403	0.554	0.794	0.683	0.499	0.428
046462	0.056	0.151	0.240	0.222	0.331	0.304	0.243	0.166
046463	0.264	0.294	0.373	0.473	0.550	0.505	0.334	0.287
046464	0.210	0.165	0.143	0.189	0.164	0.155	0.077	0.091
046551	−0.295	−0.349	−0.460	−0.450	−0.573	−0.545	−0.366	−0.293
046561	0.101	0.121	0.195	−0.068	0.020	0.066	0.010	−0.046
046562	0.349	0.358	0.400	0.498	0.531	0.503	0.341	0.277
046661	0.245	0.270	0.276	0.711	0.696	0.563	0.461	0.372
046663	0.247	0.325	0.326	0.420	0.415	0.391	0.279	0.201
055551	0.166	0.165	0.132	0.493	0.456	0.357	0.299	0.277
055561	0.278	0.272	0.238	0.660	0.618	0.521	0.353	0.383
055661	0.166	0.282	0.305	0.149	0.167	0.205	0.124	0.050
056561	0.171	0.105	0.215	−0.084	0.045	0.098	−0.005	−0.001
056562	0.235	0.266	0.281	0.452	0.451	0.421	0.342	0.248
056661	−0.115	−0.074	−0.132	−0.090	−0.141	−0.142	−0.115	−0.039
066661	−0.036	0.007	−0.036	0.432	0.364	0.236	0.210	0.257
066663	0.052	0.074	0.080	0.173	0.170	0.137	0.141	0.076

energies (in MeV) are as follows: ($TJ = 01$; 0.071, 0.281, 0.224, 0.174, 0.183), ($TJ = 03$; 0.085, 0.125, 0.118, 0.072, 0.070), ($TJ = 10$; −0.340, 0.334, 0.149, 0.243, 0.315), ($TJ = 12$; 0.239, 0.504, 0.437, 0.326, 0.308). In each case the five numbers refer to (present $2\hbar\omega$, present G_{3p1h}, Fig. 7(c) compound spectra, Fig. 7(b) compound spectra, G^T_{3p1h}), respectively. Thus the converged value of the core polarization is seen to generally give a repulsive shift to the centroids relative to that of the $2\hbar\omega$ calculation. However, with the notable exception of the $TJ = 10$ case, it is found that this shift is reduced as we progressively make the transition from oscillator to plane-wave propagation for the intermediate particle. In fact the $TJ = 10$ case is the only case in which the centroid of a JT group of levels using G^T_{3p1h} does not lie well within $\frac{1}{4}$ MeV of the centroid using the pure $2\hbar\omega$ approximation for G_{3p1h}. It is in this sense that we find the VSW effect to be somewhat weakened, but none the less important, by the use of plane-wave propagation.

We conclude by presenting in Figs. 14 and 15 the obligatory spectra for ^{18}O and ^{18}F using each of the present calculations of core polarization in combination with the G-matrix elements for the

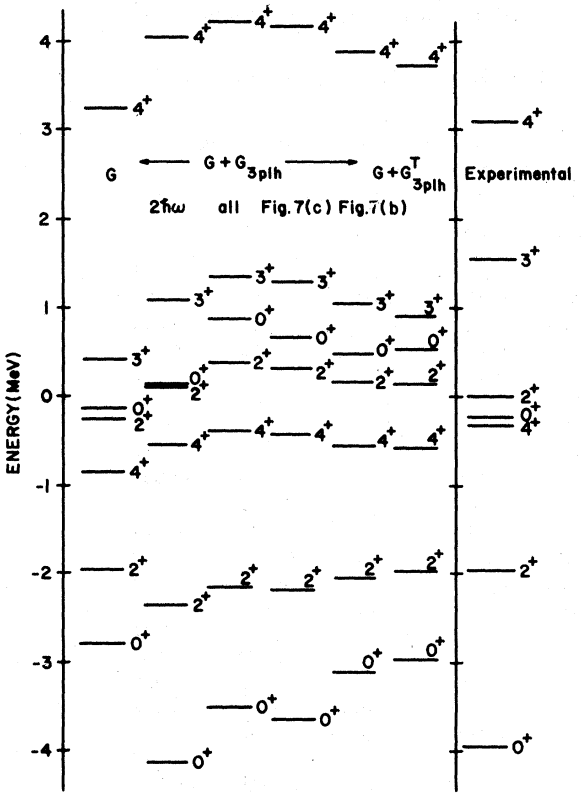

FIG. 14. The spectra of ^{18}O.

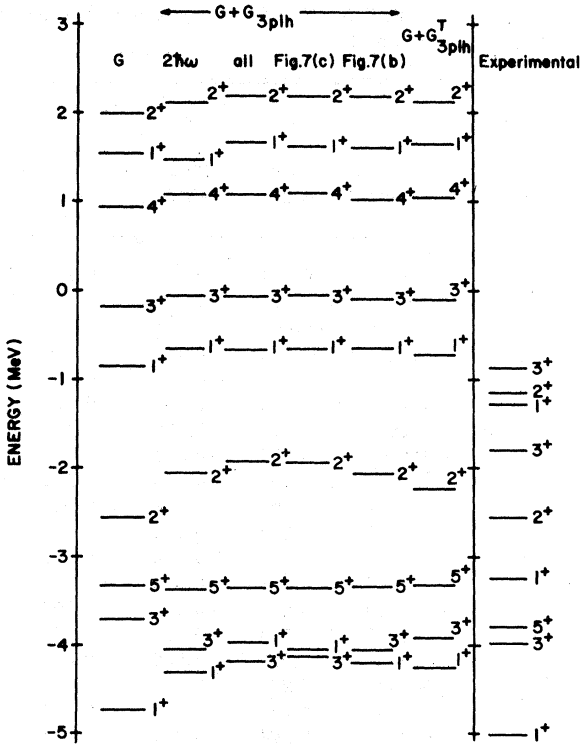

FIG. 15. The spectra of ^{18}F.

valence states to produce effective interaction matrix elements. We note merely the relative stability of the level structure against changes in the method of calculation of the core polarization. Again the $TJ = 10$ levels prove exceptional. Calculations with $2\hbar\omega$ G_{3plh} alone yield results in considerably better agreement with experiments. The inclusion of high energy particle excitations significantly reduce the overall effect of the second-order core-polarization diagram, as was found by VSW and the present work. How to amend this situation is clearly of interest and importance. There is room for the influence of higher order core-polarization processes such as exchanges of RPA phonons between valence nucleons. There is the possibility that a different nucleon-nucleon potential model, such as the Paris potential[17] and the Bonn potential,[18] may suppress the effect of these high energy particle excitations. We feel that there ought to be some mechanism which would restore the much needed core-polarization contributions to the effective nucleon-nucleon interaction in nuclei.

ACKNOWLEDGMENTS

We wish to thank Professor G. E. Brown for helpful discussions and Professor C. W. Wong for several helpful correspondences. This work was supported in part by DOE Contract No. EY-76-S-02-3001 and in part by the New York State Research Foundation.

[1]G. F. Bertsch, Nucl. Phys. 74, 234 (1965).
[2]T. T. S. Kuo and G. E. Brown, Nucl. Phys. 85, 40 (1966).
[3]G. E. Brown and T. T. S. Kuo, Nucl. Phys. A92, 481 (1967).
[4]T. T. S. Kuo, Annu. Rev. Nucl. Sci. 24, 101 (1974).
[5]P. J. Ellis and E. Osnes, Rev. Mod. Phys. 49, 777 (1977).
[6]B. R. Barrett and M. K. Kirson, Nucl. Phys. A148, 145 (1970).
[7]T. H. Schucan and H. A. Weidenmüller, Ann. Phys. (N.Y.) 73, 108 (1972).
[8]J. P. Vary, P. D. Sauer, and C. W. Wong, Phys. Rev. C 7, 1776 (1973).
[9]E. M. Krenciglowa, C. L. Kung, T. T. S. Kuo, and E. Osnes, Ann. Phys. (N.Y.) 101, 154 (1976).
[10]B. R. Barrett, R. G. L. Hewitt, and R. J. McCarthy, Phys. Rev. C 3, 1137 (1971).
[11]C. W. Wong, Nucl. Phys. A91, 399 (1967).

[12]M. Baranger, in *Nuclear Structure and Nuclear Reactions*, in *Proceedings of the International School of Physics "Enrico Fermi," Course XL*, edited by M. Jean and R. A. Ricci (Academic, New York, 1969), p. 511.
[13]J. Shurpin, H. Müther, T. T. S. Kuo, and A. Faessler, Nucl. Phys. A293, 61 (1977).
[14]R. Balian and E. Brezin, Nuovo Cimento 61B, 403 (1969).
[15]C. W. Wong and D. M. Clement, Nucl. Phys. A183, 210 (1972).
[16]S. F. Tsai and T. T. S. Kuo, Phys. Lett. 39B, 427 (1972).
[17]R. Vinh Mau, in *Mesons in Nuclei*, edited by M. Rho and D. Wilkinson (to be published).
[18]K. Erkelenz, K. Holinde, and K. Bleuler, Nucl. Phys. A139, 308 (1969); K. Holinde and R. Machleidt, Nucl. Phys. A247, 495 (1975).